LWT - Food Science and Technology 182 (2023) 114820

Contents lists available at ScienceDirect

LWT

journal homepage: www.elsevier.com/locate/lwt

High virulence *Proteus mirabilis* strains cause acceleration of decay of fresh-cut fruits

Lanhua Yi [a,b,1], Ping Zeng [c,1], Jitao Tang [a], Junhe Ren [a], Kaifang Zeng [a,**], Sheng Chen [b,d,*]

[a] College of Food Science, Southwest University, Chongqing, 400715, PR China
[b] Department of Food Science and Nutrition, The Hong Kong Polytechnic University, Hom Hung, Kowloon, Hong Kong
[c] School of Pharmacy, Faculty of Medicine, The Chinese University of Hong Kong, Shatin, Hong Kong
[d] Department of Infectious Diseases and Public Health, Jockey Club College of Veterinary Medicine and Life Sciences, City University of Hong Kong, Kowloon, Hong Kong

ARTICLE INFO

Keywords:
Fresh-cut fruits
Proteus mirabilis
Food safety
Toxicity
HS-GC-IMS

ABSTRACT

The role of *Proteus mirabilis* on food safety has not been investigated before. Three *P. mirabilis* strains (swupm1, swupm2 and swupm3) isolated from fresh-cut fruits were shown to vary in swarming motility, with strains swupm1 and swupm2, but not swupm3 exhibiting the characteristic bull's-eye phenotype. Strains swupm1 and swupm2 grew faster and produced stronger biofilm than swupm3. These strains were all multidrug resistant and exhibited high virulence in *Galleria mellonella* (100% mortality at around 100 CFU inoculum) with swupm1 being the most virulent one. *P. mirabilis* was shown to be able to survive in fresh-cut cantaloupe at 4 °C and facilitate the growth of other bacteria. At 25 °C, *P. mirabilis* could significantly accelerate the decay of fresh-cut fruits. Headspace gas chromatography–ion mobility spectrometry (HS-GC-IMS) analysis showed that *P. mirabilis* strain swupm1 could cause dramatic changes in the volatile components of fresh-cut cantaloupe, such as ethyl acetate, ethanol and formic acid. This study indicates that *P. mirabilis* can accelerate the decay of fresh-cut fruits and that the virulence level of these strains seems to be closely associated with the adverse effect of such strains on food quality.

1. Introduction

Proteus mirabilis widely exists in the natural environment and is found in abundance in water, soil and the gastrointestinal tract of human and animals. It can cause a variety of human infections at the wounds, eyes, gastrointestinal tract and urinary tract (Armbruster, Mobley, & Pearson, 2018). Acute *P. mirabilis* infections may lead to cystitis, pyelonephritis, urolithiasis, sepsis and septic shock (Debnath et al., 2018). Urinary tract infection (UTI), especially catheter associated urinary tract infections (CAUTI), is a highly concerned issue in hospitals. In the USA, *P. mirabilis* accounts for about 3% of all hospital infections and 44% of CAUTI (Yuan et al., 2021). The pathogenicity of *P. mirabilis* is associated with production of virulence factors, such as adhesins, ureases, proteases, siderophores, various toxins, and those involved in invasion and formation of biofilm. The ability to swim in liquid medium and the swarming motility on solid surface further facilitate rapid transmission of this pathogen.

Although *P. mirabilis* is a well-known opportunistic pathogen resulting in nosocomial infections, it also can cause food poisoning with the typical symptoms of diarrhea or vomiting. For example, outbreaks of food poisoning caused by *P. mirabilis* were reported in Shenzhen (Gong, Bai, Ng'ambi, Shi, & Cao, 2018) and in Beijing (Wang et al., 2010), China. Psychrotrophic *P. mirabilis* strains were mostly isolated from meat products and seafood products (Jiang et al., 2017; Yeh, Line, & Hinton, 2018). Sanches et al. (2021) reported that *P. mirabilis* from meat samples exhibited similar genetic characteristics and identical virulence profiles when compared to those from CAUTI. Moreover, *P. mirabilis* exhibit intrinsic resistance to polymyxin, nitrofurantoin, and tetracycline (de Oliveira et al., 2021), rendering treatment of infection caused by this pathogen difficult. Therefore, *P. mirabilis* in food is regarded as an emerging threat to public health. Compared with meat products, fresh-cut fruits may pose even higher safety risk, because they are consumed without any sterilization procedures to remove *P. mirabilis*. However, effects of *P. mirabilis* on the safety and quality of fresh-cut fruit

* Corresponding author. Department of Food Science and Nutrition, The Hong Kong Polytechnic University, Hom Hung, Kowloon, Hong Kong.
** Corresponding author.
E-mail addresses: zengkaifang@hotmail.com (K. Zeng), sheng.chen@polyu.edu.hk (S. Chen).
[1] Contributed equally to this work and should be regarded as co-first author.

https://doi.org/10.1016/j.lwt.2023.114820
Received 26 February 2023; Received in revised form 24 April 2023; Accepted 28 April 2023
Available online 17 May 2023

are rarely documented.

In our previous study, we found that the prevalence of *P. mirabilis* in fresh-cut fruit is very high. We then selected three strains, swupm1, swupm2 and swupm3, that exhibited different genotypic and phenotypic characteristics, as representative strains for analysis in this study. The objectives of this work were to investigate the effects of *P. mirabilis* strains on the safety and quality of fresh-cut fruits, and elucidate the virulence genes of *P. mirabilis* strains through genomic analysis.

2. Materials and methods

2.1. Swarming motility

P. mirabilis strains swupm1, swupm2 and swupm3 were cultured overnight, and then respectively inoculated into the center of LB agar plates (1.5% agar, Invitrogen, USA) using an inoculating loop. Plates were incubated at 37 °C. At different timepoints (0, 6, 12, 24, 36, and 48 h), the radius of swarming cycles for each strain were measured using a ruler.

2.2. Construction of growth curve and scanning electron microscopy (SEM)

Overnight-cultured *P. mirabilis* strains were respectively inoculated into LB broth (1%) and incubated at 37 °C (250 rpm) for 24 h. At each hour, sample was collected and OD_{600nm} was measured on a spectrophotometer (HACH DR3900, USA). At the same time, cells of each *P. mirabilis* strain were collected at 24th h by centrifugation (6000 rpm, 10 min, 4 °C) and fixed by 2.5% glutaraldehyde (Sigma, USA) overnight at 4 °C. Upon dehydration using ethanol (different concentrations from 10% to 100%), cells were dried and covered with gold particles. Cell morphology was observed in a Scanning Electron Microscope (Tescan VEGA3).

2.3. Biofilm formation

Biofilm formation of *P. mirabilis* was measured in 96-well plates using crystal violet and SYTO9/PI respectively as described by Filipiak et al. (2020), with some modifications. *P. mirabilis* strains were cultured in LB broth to $OD_{600nm} = 0.1$, and then respectively transferred into wells of 96-well plates after double dilution (200 μL/well). During a period of 7 days, cells in the wells were removed and biofilm attached to wells was measured using crystal violet (ThermoFisher, USA) staining under 595 nm every day. At the same time, biofilm on the bottom of wells of 96-well plates on the third day was stained with SYTO9/PI solution according to the manufacturer's protocol (Live/Dead *Bac*Light Bacterial Viability kit, ThermoFisher, USA). Treated biofilm was photographed on a live-cell fluorescence imaging system (Eclipse Ti2, Nikon, Japan).

2.4. Detection of antibiotic resistance

Antibiotic resistance of three *P. mirabilis* strains was measured using the broth dilution method according to guidelines of the Clinical and Laboratory Standards Institute (CLSI) (Yi et al., 2022). The following antibiotics were tested: ampicillin, gentamicin, chloramphenicol, ciprofloxacin, norfloxacin; these five antibiotics were purchased from Sigma, USA; amikacin, colistin, ceftazidime, cefoperazone, meropenem, tetracycline, tigecycline were purchased from Meilunbio, China. *Escherichia coli* ATCC25922 was used as a quality control strain.

2.5. In vivo toxicity tests

Log-phase cells of the three *P. mirabilis* strains were collected and resuspended in sterile cantaloupe juice until a final concentration of 10^5, 10^4, 10^3, and 10^2 CFU/mL was reached. The suspension was passed through 0.22 μm filter to remove debris in the juice. A 10 μL suspension of each *P. mirabilis* strain was injected into the proleg of *Galleria mellonella* larvae. Survival ratio of larvae was monitored every 12 h. Larvae that did not respond to physical stimulation and exhibited black pigmentation were regarded as dead. Sterile cantaloupe juice without *P. mirabilis* was used as the control.

2.6. Effect of P. mirabilis on the quality of fresh-cut cantaloupe upon storage

Three *P. mirabilis* strains were cultured to log-phase. Cells were respectively collected by centrifugation (6000 rpm, 10 min, 4 °C) and resuspended in sterile saline until a cell concentration of 10^5 CFU/mL was reached. Fresh cantaloupe was peeled and cut into pieces (about 2 cm × 3 cm). Fresh-cut cantaloupe was dipped in prepared *P. mirabilis* suspension (cantaloupe/suspension ratio = 1:6) for 5 min, then taken out and dried at room temperature. Treated fresh-cut cantaloupe was packaged in boxes and stored at 4 °C and 25 °C, respectively. Each day, sensory quality of fresh-cut cantaloupe was recorded by taking pictures. On the 7th day, samples (40 g) stored at 4 °C were taken out, ground using a mortar (LICHEN, China) in 20 mL sterile saline, and then diluted and spread onto LB plates. Colonies of *P. mirabilis* and total bacteria were counted after incubating at 37 °C for 24 h. On the 3rd day, exudate volume of samples at 25 °C was measured, as well as colonies of *P. mirabilis* and total bacteria in exudate were counted after treatment as described above. Fresh-cut cantaloupe subjected to the same treatment but without *P. mirabilis* was included as control.

2.7. Headspace gas chromatography–ion mobility spectrometry (HS-GC-IMS) analysis of fresh-cut cantaloupe

Fresh-cut cantaloupe samples of control and those treated with *P. mirabilis* strain swupm1 and stored at 25 °C for two days were subjected to measurement of volatile components using HS-GC-IMS under the positive ion mode as described by Guo, Zhao, Ma, Wang, and Wang (2022). Specifically, 5 g of sample were placed in a 20 mL headspace bottle and incubated at 50 °C for 15 min. Then, 500 μL headspace gas was injected into a MXT-5 capillary column (15 mL, 0.53 mm ID, 1 μm FT). The sample was separated by nitrogen as the carrier gas at a flow rate of 150 mL/min. Running time was 20 min as follows: 2 mL/min for 2 min, then a linear rise from 2 mL/min to 100 mL/min in 18 min. Volatile compounds were analyzed using an IMS instrument (FlavourSpec®, Germany) and identified by matching the retention index (RI) and the drift time, using the standard in the GC-IMS library (Shandong Hanon Scientific Instruments Co., Ltd, China).

2.8. Complete genome sequencing and comparative genome analysis

Complete genome sequencing of the three *P. mirabilis* strains was performed by means of a combination of Illumina HiSeq sequencing and MinION nanopore sequencing as described in our previous study (Yi, Qi, Hong, Deng, & Zeng, 2020). Log-phase cells of *P. mirabilis* were subjected to genomic DNA extraction according to the instruction of the PureLink® Genomic DNA Mini Kit (Invitrogen, USA). Pair end (2 × 150 bp) library was prepared using the NEB Next® Ultra™ DNA Library Prep Kit for Illumina (NEB, USA), following the manufacturer's guidelines. The DNA libraries were sequenced in the Illumina HiSeq4000 platform and 150 bp paired-end reads were generated. DNA library of MinION nanopore sequencing was prepared using the Rapid Barcoding Sequencing Kit (SQK-RBK001, Oxford Nanopore, UK), according to manufacturer's protocol. The DNA library was loaded into the Flow Cell (R9.4.1) in a MinION device and sequenced by using the MinKNOW1.5.12 software. Assembly of short reads from Illumina sequencing and long reads from MinION nanopore sequencing was carried out by using the Unicycler software (Wick, Judd, Gorrie, & Holt, 2017).

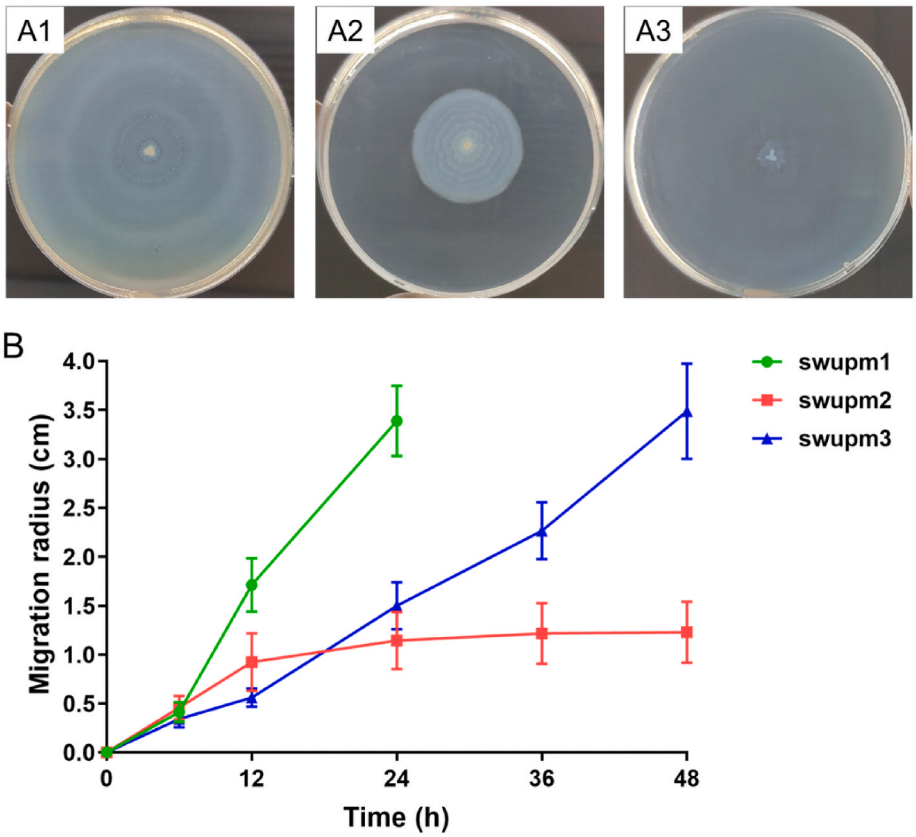

Fig. 1. Swarming motility phenotypes of three *P. mirabilis* strains (A) and their swarming motility speeds (B). (A1) Swarming motility phenotype of *P. mirabilis* swupm1; (A2) swarming motility phenotype of *P. mirabilis* swupm2; (A3) swarming motility phenotype of *P. mirabilis* swupm3.

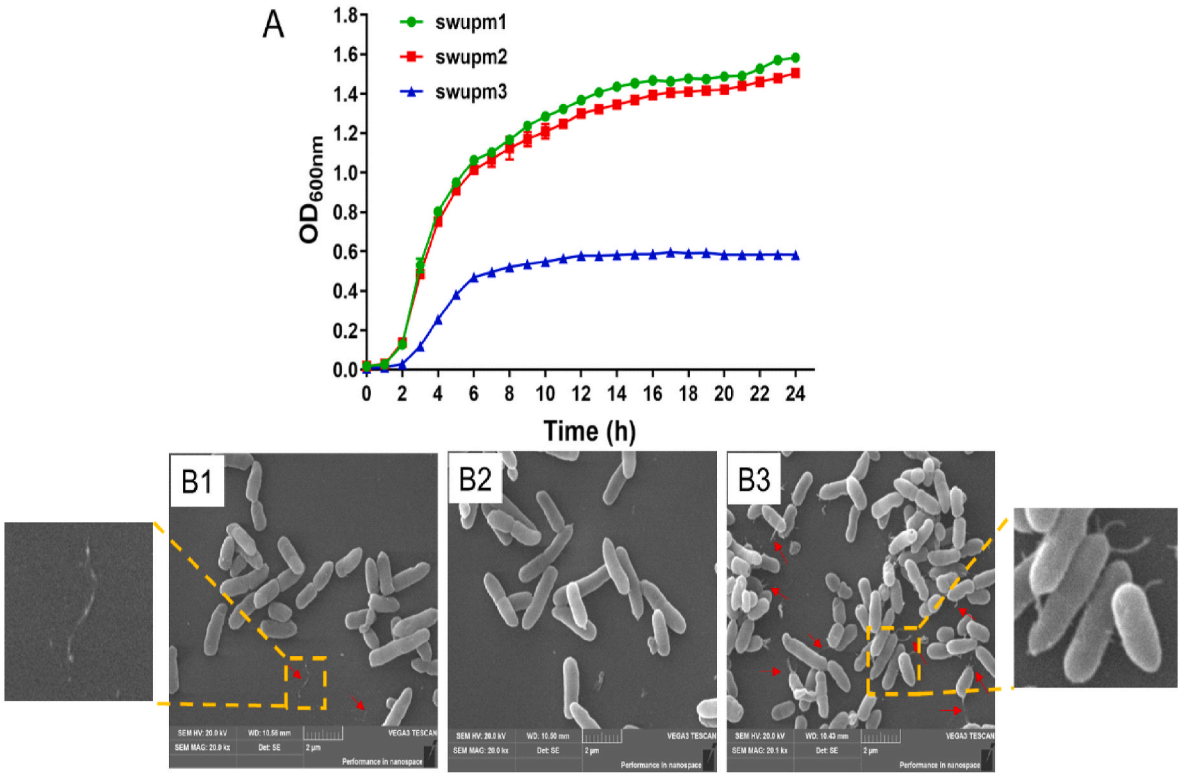

Fig. 2. Growth curves (A) and SEM images (B) of three *P. mirabilis* strains. (B1) SEM image of *P. mirabilis* swupm1; (B2) SEM image of *P. mirabilis* swupm2; (B3) SEM image of *P. mirabilis* swupm3.

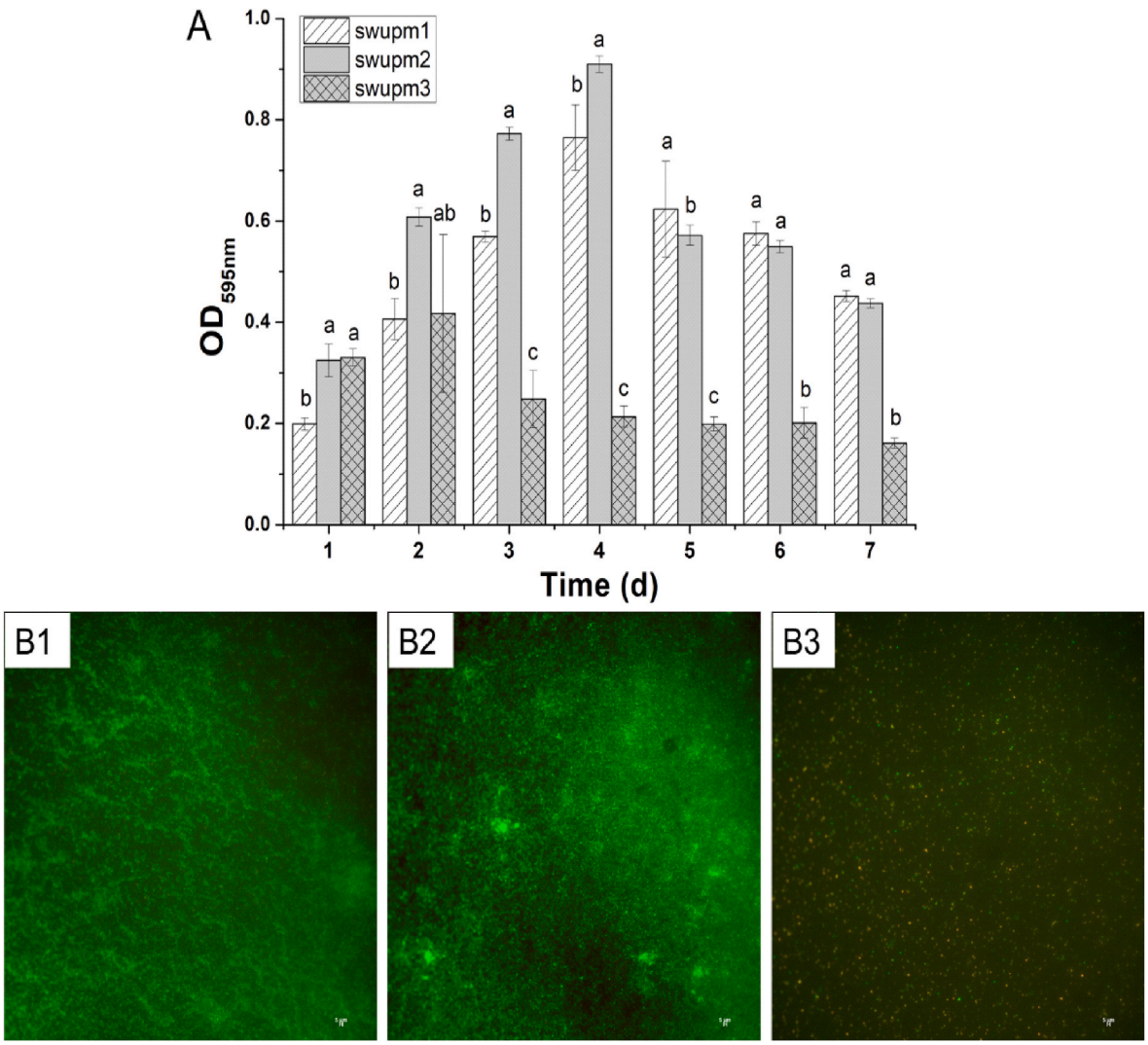

Fig. 3. Biofilm formation of three *P. mirabilis* strains. (A) Biofilm formation during a period of 7 days of three *P. mirabilis* strains analyzed by crystal violet; (B1) biofilm formation of *P. mirabilis* swupm1 on the 3rd d observed by fluorescence microscope; (B2) biofilm formation of *P. mirabilis* swupm2 on the 3rd d observed by fluorescence microscope; (B3) biofilm formation of *P. mirabilis* swupm3 on the 3rd d observed by fluorescence microscope. Different letters above the bars indicated significant differences of the three strains on a same day. (For interpretation of the references to colour in this figure legend, the reader is referred to the Web version of this article.)

Gene annotation was performed by using RAST (http://rast.nmpdr.org/). Average nucleotide identity (ANI) was analyzed by using the ANI calculator (http://enve-omics.ce.gatech.edu/ani/). The cyclic images and a comparative genomic analysis were generated using CDView (http://stothard.afns.ualberta.ca/cgview_server/), BLAST Ring Image Generator (BRIG), and OrthoVenn2 (https://orthovenn2.bioinfotoolkits.net/home), in which a reference genome of *P. mirabilis* strain HI4320 (GenBank assembly accession: GCA_000069965.1) was downloaded from NCBI. Antibiotic resistance genes were identified using ResFinder 4.1 (https://cge.cbs.dtu.dk/services/ResFinder/).

2.9. Statistical analysis

All experiments were performed in triplicate. The results were expressed as mean ± standard deviation. SPSS 23.0 (IBM, USA) was used to perform statistical analysis. Evaluation of significance in statistical difference was performed by ANOVA and t-tests. A P value of <0.05 was considered statistically significant.

3. Results and discussion

3.1. Difference in swarming motility of the three P. mirabilis test strains

Although *P. mirabilis* strains swupm1, swupm2 and swupm3 were all isolated from fresh-cut fruits, they exhibited different colonial morphology. In addition, significant differences in swarming motility were observed among the three test strains. As shown in Fig. 1, *P. mirabilis* strain swupm1 (Fig. 1A1) and swupm2 (Fig. 1A2) exhibited the characteristic bull's-eye phenotype (Schaffer & Pearson, 2015) with terrace-like colonial morphology; such features were not observed in strain swupm3. It should be noted that *P. mirabilis* strain swupm1 could migrate a longer distance and that *P. mirabilis* strain swupm2 exhibited more consolidated colonies. However, no obvious oscillating wave was observed for *P. mirabilis* strain swupm3 (Fig. 1A3). After 48 h incubation, migration radiuses of *P. mirabilis* strains swupm1 and swupm3 were over 3 cm, but that of swupm2 was only around 1 cm (Fig. 1B). In summary, the swarming motility of these three *P. mirabilis* strains were in the order of: swupm1 > swupm3 > swupm2 such difference might be due to their differences in the ability to undergo cell proliferation as well as cellular morphology.

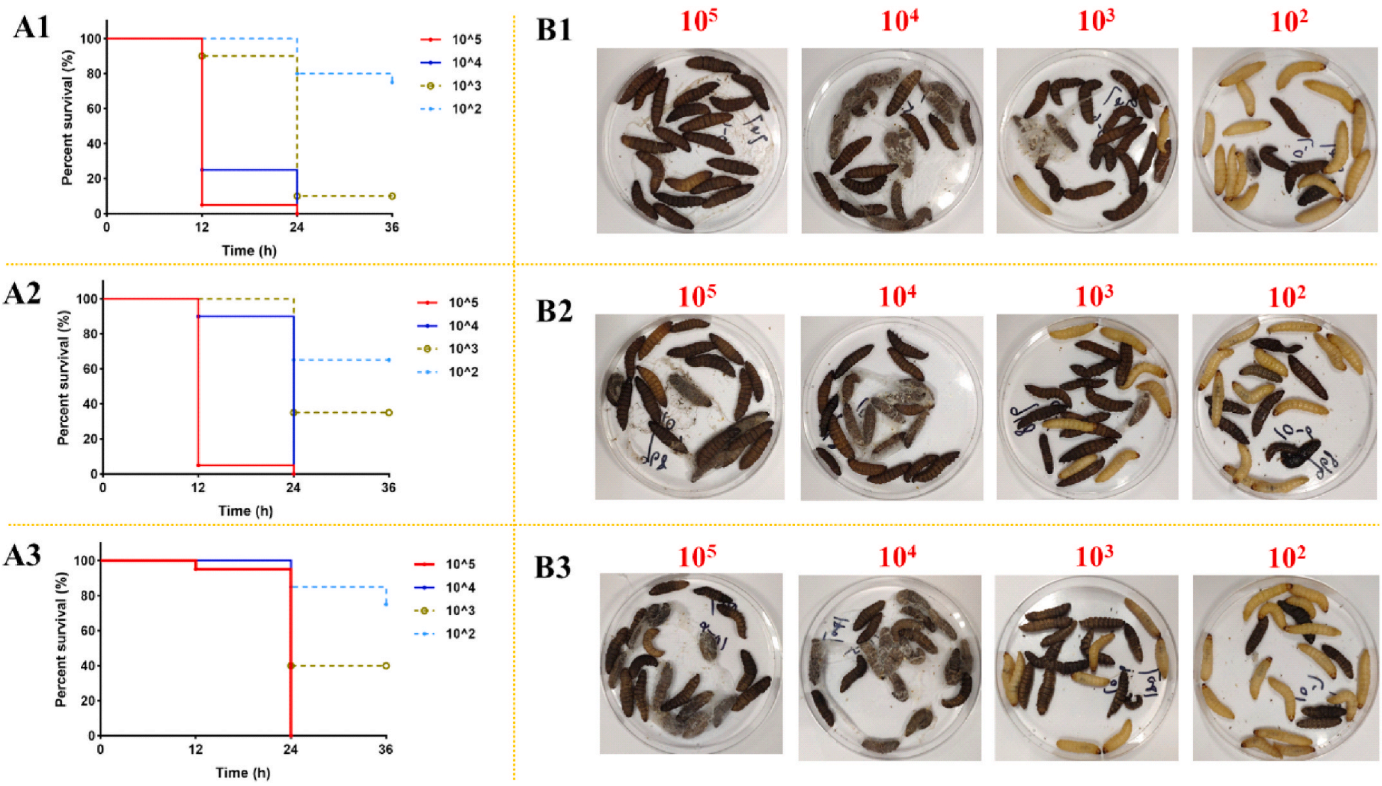

Fig. 4. The survival rate (A) and larvae phenotype at 36 h (B) of *G. mellonella* after treated by three *P. mirabilis* strains with different cell density. (A1 and B1) *P. mirabilis* swupm1 treatment; (A2 and B2) *P. mirabilis* swupm2 treatment; (A3 and B3) *P. mirabilis* swupm3 treatment.

3.2. Growth dynamics and cell morphology of three P. mirabilis strains

The growth dynamics and cell morphology of the three *P. mirabilis* strains were analyzed and shown in Fig. 2. The three *P. mirabilis* strains exhibited typical growth curves with lag-phase (0–2 h), log-phase (2–6 h), and stationary-phase (6–24 h) observable during the period of 24 h OD_{600nm} values of *P. mirabilis* swupm1 and swupm2 were found to overlapped at various time points but were significantly higher than that of swupm3 (Fig. 2A). During the stationary-phase, slow increase in OD_{600nm} value was observed for *P. mirabilis* strains swupm1 and swupm2. The higher absorbance and the subsequent slow increase in absorbance in these two strains may be related to the formation of biofilm.

Different growth dynamics of the three *P. mirabilis* strains may be closely related the differences in cellular morphology. Therefore, their cellular morphology was observed using SEM. As shown in Fig. 2B, *P. mirabilis* strains swupm1, swupm2, and swupm3, were rod-shape and about 1–3 μm in length. The proportion of cells with short cell length was higher in strain swupm3 than the other two strains. Lee and Belas (2015) reported that *P. mirabilis* cells were 1.5–2.0 μm swimmer cells with 4–6 flagella when in liquid. In LB broth, the three *P. mirabilis* strains had approximate cell length. However, only *P. mirabilis* swupm3 had flagella (red arrows in Fig. 2B3). Flagella were also found on glass slide beside the *P. mirabilis* swupm1 cells (red arrows in Fig. 2B1), which might have fallen off the cells during the handling process. According to images of SEM, *P. mirabilis* strain swupm2 had the lowest number of flagella. We speculated that this might be a reason of the slow swarming rate of this strain.

3.3. Biofilm formation of the three P. mirabilis strains

Biofilm formation is an inherent property of *P. mirabilis* (Lin et al., 2022). The result of the growth dynamics experiment as described above indicates that there may be differences in biofilm formation among the three *P. mirabilis* strains. We found that the biofilm biomass of the three *P. mirabilis* strains increased first, and then decreased, exhibiting the same trend as illustrated in Fig. 3A. However, the highest biomass of biofilm of the three strains occurred at different times. Biomass of biofilm reached the highest level on the 4th day for *P. mirabilis* strains swupm1 and swupm2, but that of *P. mirabilis* strain swupm3 reached the highest level on the 2nd day. The maximum degree of biofilm accumulation also varied significantly: swupm2 > swupm1 > swupm3. Biofilm formation potential of *P. mirabilis* swupm3 was dramatically weaker than that of the other two strains. This finding was in line with the measured absorbance in growth curve (Fig. 2A). Generally, motility and biofilm formation are mutually exclusive (Lee & Belas, 2015). This pattern can be observed between *P. mirabilis* swupm2 and swupm3. *P. mirabilis* strain swupm2 has weak swarming motility but strong biofilm formation capability; for *P. mirabilis* strain swupm3, the opposite was observed. Interestingly, *P. mirabilis* strain swupm1 has both strong swarming motility and strong biofilm formation potential. We speculated that the biofilm structure of *P. mirabilis* strain swupm1 may contribute to a high swarming motility.

Furthermore, the biofilm morphology of the three *P. mirabilis* strains was observed by fluorescence microscope. As shown in Fig. 3B, the biofilm formed by *P. mirabilis* strain swupm1 presented the morphology of vibrating water with ripples (Fig. 3B1), while the appearance of swupm2 biofilm exhibited stacked clouds, with different tightness and thickness (Fig. 3B2). Both *P. mirabilis* strains swupm1 and swupm2 had rich biofilm, but biofilm of swupm1 was flat without pileup. This flat characteristic may not prevent motility of swupm1 and actually results in strong swarming motility. Compared with *P. mirabilis* strains swupm1 and swupm2, the biofilm of swupm3 was very thin. Dotted individual cells could be clearly visualized (Fig. 3B3). Red fluorescence could be detected in some *P. mirabilis* swupm3 cells, indicating that they had died on the third day. According to Fig. 3A, biofilm of *P. mirabilis* strain swupm3 decreased since the third day, which might be associated with cell death and biofilm dissipation. Like catheter blockage in patient, the

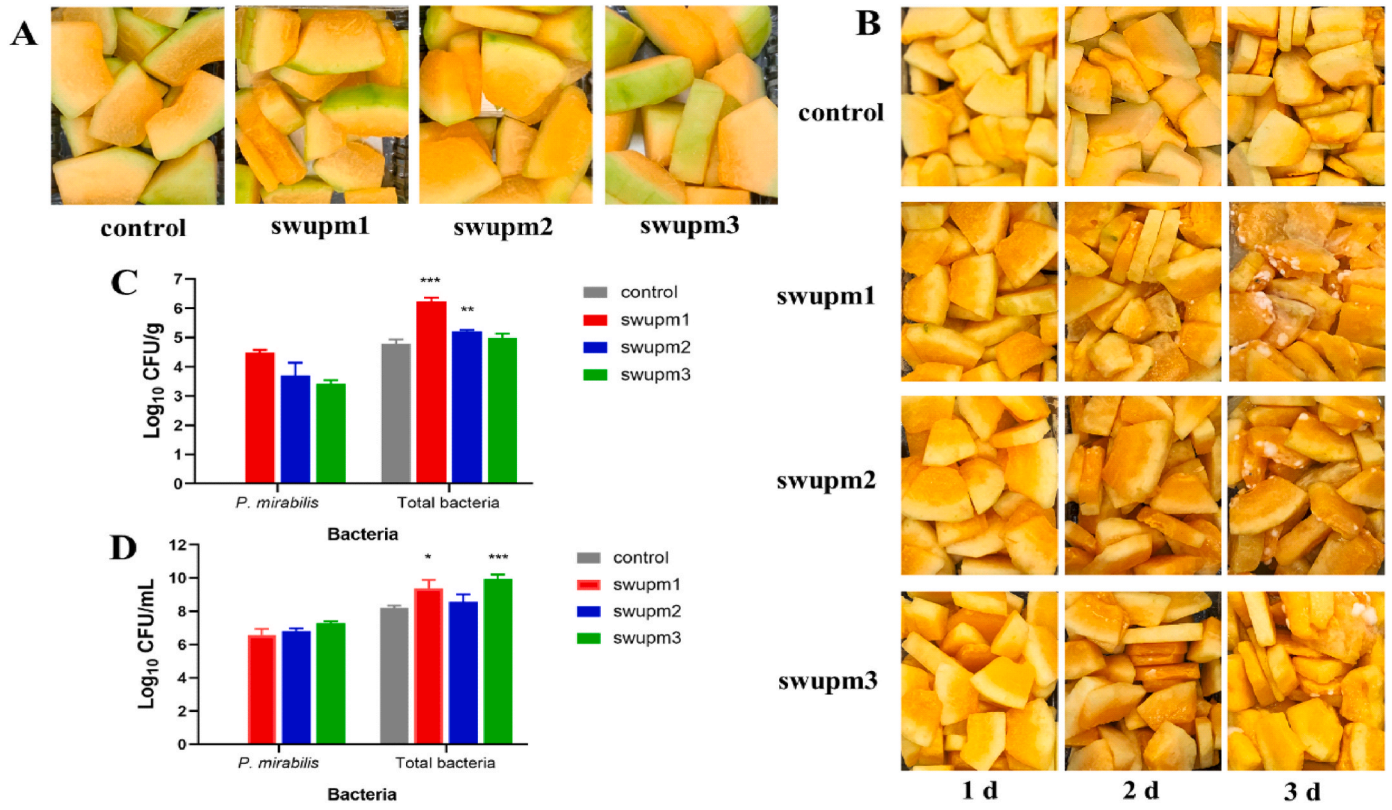

Fig. 5. Sensory quality (A, B) and bacterial quantity (C, D) of fresh-cut cantaloupe after treatment with *P. mirabilis*. (A) Sensory quality of fresh-cut cantaloupe after storage at 4 °C for 7 d; (B) sensory quality of fresh-cut cantaloupe stored at 25 °C for 1, 2, and 3 d; (C) bacterial quantity of fresh-cut cantaloupe after storage at 4 °C for 7 d; (D) bacterial quantity of exudate of fresh-cut cantaloupe after storage at 25 °C for 3 d * indicated significant difference at the $P < 0.05$ level, ** indicated significant difference at the $P < 0.01$ level, *** indicated significant difference at the $P < 0.001$ level, they were compared with the control.

surface-associated swarming motility and the biofilm formation of *P. mirabilis* (O'May, Amzallag, Bechir, & Tufenkji, 2016) may lead to aggravated pollution and blockage of processing equipment of fresh-cut food samples.

In summary, the three *P. mirabilis* strains have different degrees of swarming, which is closely associated with growth rate, flagella number, biofilm formation potential, and biofilm morphology. It is most likely that the swarming motility and biofilm formation of *P. mirabilis* may contribute to its survival and spread in food samples.

3.4. Antibiotic resistance of the three P. mirabilis strains

The antibiotic resistance result showed that all the three *P. mirabilis* strains exhibited resistance to tetracycline (MIC ≥32 μg/mL) and colistin (MIC ≥64 μg/mL). *P. mirabilis* strain swupm1 was resistant to amikacin (MIC = 32 μg/mL), cefoperazone (MIC = 64 μg/mL), meropenem (MIC = 16 μg/mL) and gentamicin (MIC = 8 μg/mL). *P. mirabilis* strain swupm2 exhibited resistance to tigecycline (MIC = 8 μg/mL). *P. mirabilis* strain swupm3 exhibited resistance to ciprofloxacin (MIC = 4 μg/mL) and norfloxacin (MIC = 16 μg/mL). The sustained development of drug resistance in *P. mirabilis* poses a severe threat to food safety (Durgadevi et al., 2019) as resistant strains render it difficult to treat patients of food poisoning.

3.5. In vivo toxicity of the three P. mirabilis strains

G. mellonella model has been widely used to evaluate the toxicity of pathogens or antimicrobial drugs (Banville, Browne, & Kavanagh, 2012) and is thereby employed to evaluate the *in vivo* toxicity of the three *P. mirabilis* strains in this study. Cantaloupe juice without *P. mirabilis* (control) exhibited no toxicity to *G. mellonella* with 100% survival rate recorded after incubation for 36 h (image is not shown). However, death rate of *G. mellonella* rose upon increase in *P. mirabilis* cell density (Fig. 4). For 10^5 CFU/mL cell density treatment, *P. mirabilis* strain swupm1, swupm2, and swupm3 respectively caused 95%, 95%, and 5% death at 12 h; the death rate then increased to 100% in all experiments at 24 h. For 10^4 CFU/mL cell density treatment, *P. mirabilis* strain swupm1 exhibited a higher fatality rate at 12 h, but the death rate of *G. mellonella* again reached 100% in all experiments at 24 h. For 10^3 CFU/mL cell density treatment, *P. mirabilis* strain swupm1 exhibited the highest level of toxicity, with death rate of 90% at 36 h, followed by *P. mirabilis* strain swupm2 (65% death rate) and *P. mirabilis* strain swupm3 (60% death rate). For 10^2 CFU/mL cell density treatment for 36 h, the *P. mirabilis* strains still caused 25%–35% death of *G. mellonella*. In short, *P. mirabilis* swupm1 exhibited acute toxicity to *G. mellonella*, followed by *P. mirabilis* strain swupm2 and then *P. mirabilis* strain swupm3. All the three *P. mirabilis* strains could cause 100% death of *G. mellonella* at cell density ≥ 10^4 CFU/mL (100 bacteria/insect).

As shown in Fig. 4, the three *P. mirabilis* strains exhibited LD_{50} values ranging from 2 $\log_{10}$ CFU/mL to 3 $\log_{10}$ CFU/mL, which were within the range of 2–3.9 $\log_{10}$ CFU/mL (1–40 bacteria/insect) reported by Chadwick (1971). The LD_{50} values of most *Pseudomonas aeruginosa* strains ranged from 2 to 20 bacteria/insect (Chadwick, 1967). The common foodborne pathogen *Salmonella* has LD_{50} values of 10^2–10^3 bacteria/insect (Fpds et al., 2021; Freitas, Silva, Fernandes, Carneiro, & Vanetti, 2021). The low LD_{50} value of *P. mirabilis* indicates that it has strong toxicity, posing a significant threat to food safety.

3.6. Effect of P. mirabilis on the storage quality of fresh-cut cantaloupe

P. mirabilis widely exists in fresh-cut fruit, however, its effects on the sensory quality and bacterial quantity of fresh-cut fruit are unclear. As

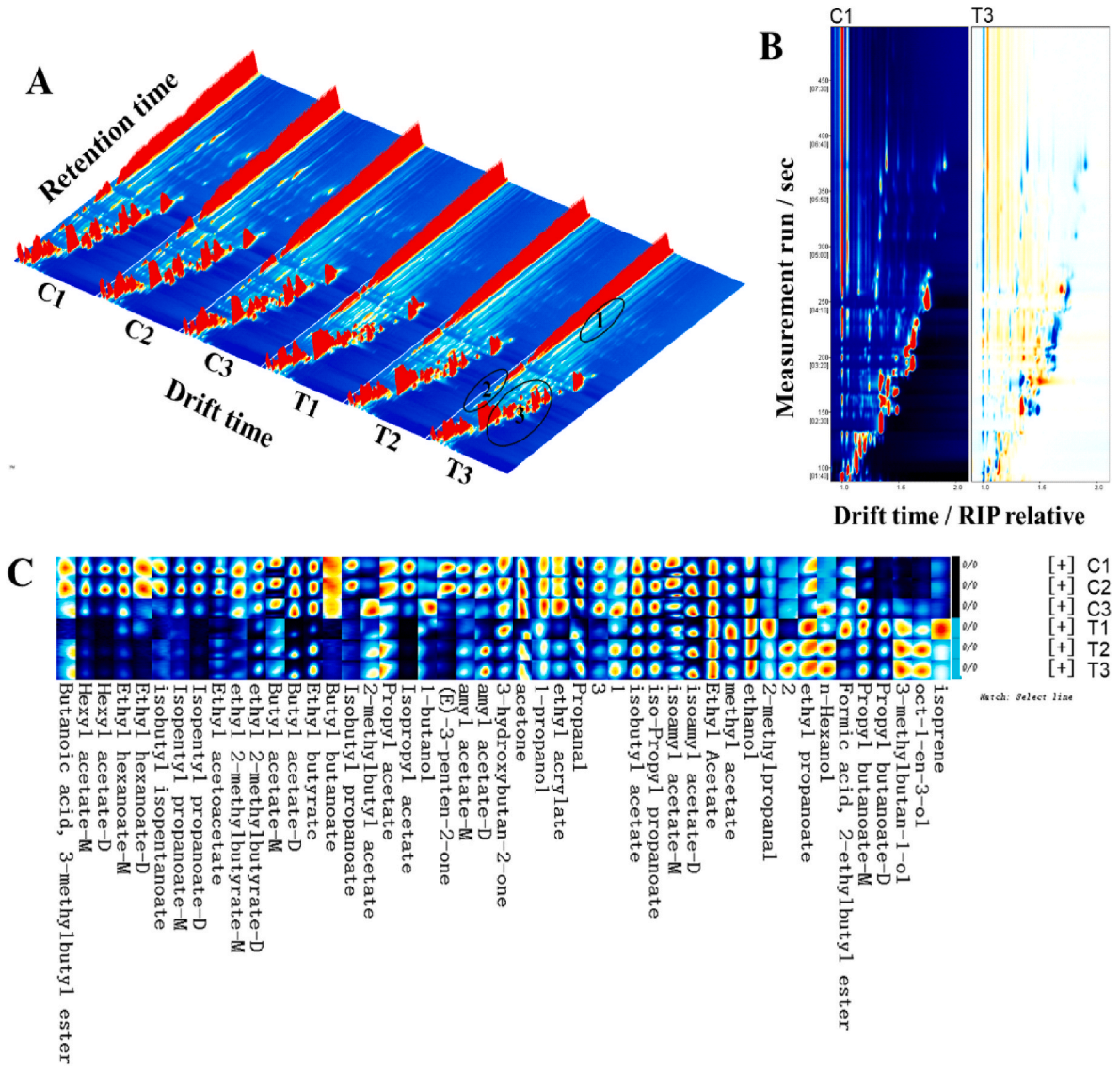

Fig. 6. Volatile components analysis of fresh-cut cantaloupe by HS-GC-IMS. (A) 3D-topographic plots of volatile compounds in fresh-cut cantaloupe; (B) comparison difference topographic plots of volatile components in fresh-cut cantaloupe; (C) fingerprint of volatile compounds in fresh-cut cantaloupe. C1, C2, and C3 was abbreviation of control 1, control 2, and control 3, respectively; T1, T2, and T3 was abbreviation of *P. mirabilis* swupm1 treatment 1, *P. mirabilis* swupm1 treatment 2, and *P. mirabilis* swupm1 treatment 3, respectively.

shown in Fig. 5A, after 4 °C storage for 7 d, sensory quality of fresh-cut cantaloupe between the three *P. mirabilis* strains treatments and control was almost the same. There was no unpleasant smell for all treatments. At the same time, colonies of *P. mirabilis* in fresh-cut cantaloupe samples were around 10^4 CFU/g (Fig. 5C), which were close to that of the initial inoculum. Fresh-cut fruits are usually kept at low temperature (2–8 °C). Therefore, this storage condition is considered effective. Unfortunately, total bacteria of fresh-cut cantaloupe treated with *P. mirabilis* strains swupm1 and swupm2 were significantly higher than that of the control. The results indicate that *P. mirabilis* can survive in fresh-cut cantaloupe at 4 °C and the existence of *P. mirabilis* may result in significant increase in the total bacterial population in fresh-cut fruits.

In comparison with the effect of storage at 4 °C, storage at room temperature (25 °C) resulted in significant change in the sensory quality of fresh-cut cantaloupe (Fig. 5B). Fruits in the control group almost maintained the same texture during the first two days. Maceration was observed in partial fruit tissue on the third day. However, for *P. mirabilis* treatments, tissue maceration was observed in all pieces of fresh-cut cantaloupe on the first day. On the second day, rotten tissue coved by mucus was observed, with concomitant obvious exudate and the sour smell. On the third day, exudate volume increased to 11.3 ± 0.18, 6.9 ± 1.98, 10.9 ± 0.10 mL/100 g fruit for samples treated with *P. mirabilis* strains swupm1, swupm2 and swupm3, respectively, while that of control was 4.5 ± 1.06 mL/100 g fruit. Moreover, the surface of some fruit was covered with white flocculent mold, especially the fruit samples treated by *P. mirabilis* swupm1. The serious decay of fruit reminds us to avoid exposure of fresh-cut fruits at room temperature during processing, storage, distribution, and sale. Worse still, *P. mirabilis* contamination was found to accelerate the decay. The number of *P. mirabilis* in fresh-cut cantaloupe exudate increased to around 10^7 CFU/mL (Fig. 5D) on the third day. Compared with the control, the total bacteria of fresh-cut cantaloupe exudate also increased after *P. mirabilis* treatment. No matter at low temperature or room temperature, existence of *P. mirabilis* enhanced the growth of other bacteria. This phenomenon may be due to degradation the fruit products caused by *P. mirabilis*, thereby providing better nutrition for the growth of other bacteria.

Table 1
Effect of *P. mirabilis* on volatile compounds in fresh-cut cantaloupe identified by HS-GC-IMS.

No.	Compound	CAS#	Formula	MW	RI	Rt [sec]	Dt [a.u.]	PV of control	PV of *P. mirabilis*
1	Butanoic acid	C109193	$C_9H_{18}O_2$	158.2	1058.7	435.409	1.394	143.37 ± 18.67	106.61 ± 43.90
2	Hexyl acetate-M[a]	C142927	$C_8H_{16}O_2$	144.2	1016.3	374.456	1.392	1400.84 ± 433.81	382.08 ± 60.45 ↓*
3	Hexyl acetate-D[b]	C142927	$C_8H_{16}O_2$	144.2	1015.4	373.09	1.904	710.48 ± 342.24	84.49 ± 20.81 ↓*
4	Ethyl hexanoate-M	C123660	$C_8H_{16}O_2$	144.2	1002.6	354.65	1.340	941.22 ± 149.53	380.41 ± 118.60 ↓**
5	Ethyl hexanoate-D	C123660	$C_8H_{16}O_2$	144.2	1003.3	355.674	1.809	116.52 ± 56.38	37.13 ± 31.31
6	isobutyl isopentanoate	C589593	$C_9H_{18}O_2$	158.2	983.1	334.502	1.389	251.11 ± 108.62′	101.47 ± 15.57
7	Isopentyl propanoate-M	C105680	$C_8H_{16}O_2$	144.2	953.9	309.573	1.337	676.56 ± 151.22	206.78 ± 44.24 ↓**
8	Isopentyl propanoate-D	C105680	$C_8H_{16}O_2$	144.2	955.1	310.597	1.820	267.41 ± 93.20	39.06 ± 4.07 ↓*
9	amyl acetate-M	C628637	$C_7H_{14}O_2$	130.2	914.3	275.765	1.319	359.30 ± 143.93	206.90 ± 45.51
10	amyl acetate-D	C628637	$C_7H_{14}O_2$	130.2	914.3	275.765	1.766	564.58 ± 173.78	476.28 ± 222.76
11	isoamyl acetate-M	C123922	$C_7H_{14}O_2$	130.2	889.1	255.275	1.306	966.35 ± 205.71	625.06 ± 53.05 ↓*
12	isoamyl acetate-D	C123922	$C_7H_{14}O_2$	130.2	879.5	250.153	1.752	11845.64 ± 620.47	8501.35 ± 1024.08 ↓**
13	Ethyl acetoacetate	C141979	$C_6H_{10}O_3$	130.1	895.1	259.373	1.147	566.86 ± 214.71	278.93 ± 79.96
14	ethyl 2-methylbutyrate-M	C7452791	$C_7H_{14}O_2$	130.2	847.1	232.737	1.241	354.14 ± 99.33	118.81 ± 6.14 ↓*
15	ethyl 2-methylbutyrate-D	C7452791	$C_7H_{14}O_2$	130.2	844	231.09	1.656	1309.54 ± 162.62	657.30 ± 160.84 ↓**
16	Butyl acetate-M	C123864	$C_6H_{12}O_2$	116.2	807.9	211.738	1.244	760.58 ± 31.65	545.14 ± 103.64 ↓*
17	Butyl acetate-D	C123864	$C_6H_{12}O_2$	116.2	809.6	212.69	1.624	10589.54 ± 149.16	3104.92 ± 1622.84 ↓**
18	Ethyl butyrate	C105544	$C_6H_{12}O_2$	116.2	796.6	205.71	1.565	5639.84 ± 178.13	3060.54 ± 1553.19 ↓*
19	Propyl butanoate-D	C105668	$C_7H_{14}O_2$	130.2	898	261.862	1.691	868.10 ± 703.95	2520.96 ± 1040.80
20	Propyl butanoate-M	C105668	$C_7H_{14}O_2$	130.2	898	261.862	1.269	258.55 ± 183.22	447.21 ± 77.54
21	oct-1-en-3-ol	C3391864	$C_8H_{16}O$	128.2	983.1	334.466	1.164	40.02 ± 27.93	127.09 ± 9.81 ↑**
22	Butyl butanoate	C109217	$C_8H_{16}O_2$	144.2	1000.8	352.131	1.832	27.71 ± 2.06	7.24 ± 1.14 ↓***
23	Isobutyl propanoate	C540421	$C_7H_{14}O_2$	130.2	863.4	241.507	1.278	83.72 ± 31.35	46.23 ± 2.41
24	1	unidentified	*	0	869.4	244.693	1.689	144.72 ± 48.53	169.76 ± 16.25
25	Formic acid	U367922	$C_7H_{14}O_2$	130.2	907.9	270.323	1.289	141.60 ± 25.19	98.66 ± 54.88
26	2-methylbutyl acetate	C624419	$C_7H_{14}O_2$	130.2	898.4	262.228	1.718	290.29 ± 173.01	266.15 ± 66.75
27	2	unidentified	*	0	847.1	232.753	1.616	95.39 ± 1.11	110.11 ± 63.09
28	isobutyl acetate	C110190	$C_6H_{12}O_2$	116.2	767.8	192.404	1.621	7797.16 ± 553.36	5167.48 ± 763.47 ↓**
29	iso-Propyl propanoate	C637785	$C_6H_{12}O_2$	116.2	750.6	185.454	1.565	1464.57 ± 39.13	1181.57 ± 134.35 ↓*
30	3-methylbutan-1-ol	C123513	$C_5H_{12}O$	88.1	731.6	177.731	1.509	228.75 ± 211.51	960.29 ± 115.20 ↑**
31	Propyl acetate	C109604	$C_5H_{10}O_2$	102.1	711.2	169.451	1.485	1073.79 ± 212.98	918.12 ± 173.17
32	Isopropyl acetate	C108214	$C_5H_{10}O_2$	102.1	657	151.763	1.487	2128.12 ± 917.33	90.16 ± 42.98 ↓*
33	Ethyl Acetate	C141786	$C_4H_8O_2$	88.1	612	139.64	1.345	13988.28 ± 100.10	16247.01 ± 194.11 ↑***
34	1-butanol	C71363	$C_4H_{10}O$	74.1	690	160.855	1.370	1334.80 ± 452.53	915.61 ± 342.54
35	(E)-3-penten-2-one	C3102338	C_5H_8O	84.1	738.6	180.555	1.353	1580.21 ± 763.21	350.26 ± 47.88 ↓*
36	3-hydroxybutan-2-one	C513860	$C_4H_8O_2$	88.1	722.7	174.115	1.338	1647.32 ± 164.44	1068.79 ± 287.28 ↓*
37	2-methylpropanal	C78842	C_4H_8O	72.1	555.9	124.486	1.288	381.88 ± 48.66	476.84 ± 143.58
38	methyl acetate	C79209	$C_3H_6O_2$	74.1	536.2	119.182	1.200	2713.01 ± 630.96	3653.02 ± 752.07
39	acetone	C67641	C_3H_6O	58.1	501	109.687	1.130	5827.79 ± 37.57	4217.29 ± 969.01 ↓*
40	1-propanol	C71238	C_3H_8O	60.1	561.5	126.001	1.252	656.85 ± 12.86	522.39 ± 30.54 ↓**
41	ethanol	C64175	C_2H_6O	46.1	456	97.549	1.134	1921.69 ± 266.78	2864.49 ± 26.39 ↑**
42	ethyl acrylate	C140885	$C_5H_8O_2$	100.1	655.5	151.353	1.415	1750.68 ± 138.09	665.71 ± 296.33 ↓**
43	Propanal	C123386	C_3H_6O	58.1	513	112.924	1.162	2384.75 ± 48.70	2389.78 ± 263.78
44	3	unidentified	*	0	774.5	195.107	1.574	374.09 ± 7.03	242.56 ± 24.22 ↓***
45	ethyl propanoate	C105373	$C_5H_{10}O_2$	102.1	705.8	167.261	1.461	1002.11 ± 253.79	1646.03 ± 103.90 ↑*
46	n-Hexanol	C111273	$C_6H_{14}O$	102.2	867.6	243.745	1.640	36.58 ± 30.35	74.25 ± 10.74
47	isoprene	C78795	C_5H_8	68.1	562.3	126.23	1.215	77.07 ± 7.88	86.25 ± 21.55

a, M indicates Monomer; b, D indicates Dimer.
MW: Molecular weight, RI: the retention index, Rt: the retention time, Dt: the drift time, PV: the peak volume.
*, **, *** indicated significant difference between control and *P. mirabilis* at $P < 0.05$, $P < 0.01$, $P < 0.001$, respectively.

Table 2
General genome properties of the three *P. mirabilis* strains.

strain	Size (bp)	chromosome	plasmid	GC content (%)	CDSs	Accession No.
P. mirabilis swupm1	3,842,888	1	3	38.6	3490	CP071773
P. mirabilis swupm2	3,842,858	1	2	38.6	3491	CP071777
P. mirabilis swupm3	3,842,875	1	3	38.6	3491	CP071780

3.7. Effect of P. mirabilis on the volatile components of fresh-cut cantaloupe

According to Fig. 5, *P. mirabilis* can affect the sensory quality of fresh-cut cantaloupe with production of a sour smell. Furthermore, *P. mirabilis* strain swupm1 was used as a representative to investigate the effect of *P. mirabilis* on the volatile components of fresh-cut cantaloupe. As shown in Fig. 6A, when compared with the control, the content of some volatile components in fresh-cut cantaloupe decreased or even disappeared (circle 1 and circle 2) after *P. mirabilis* swupm1 treatment. Simultaneously, some new peaks appeared (circle 3) after treatment with *P. mirabilis* strain swupm1. Hence, *P. mirabilis* treatment leads to changes in the content and type of volatile components in fresh-cut cantaloupe. Fig. 6B provides information regarding the difference in volatile components when the control and *P. mirabilis*-treated samples were compared. Control 1 was selected as the reference with blue background. Each point represents a volatile component. If the content of a volatile component in the sample is higher than that in the reference, the point shows a red colour; otherwise, the point shows a blue colour. Compared with the reference (C1), *P. mirabilis* treatment (T3) showed many red points and blue points (Fig. 6B). It also indicates the change in content of volatile components in fresh-cut cantaloupe caused by

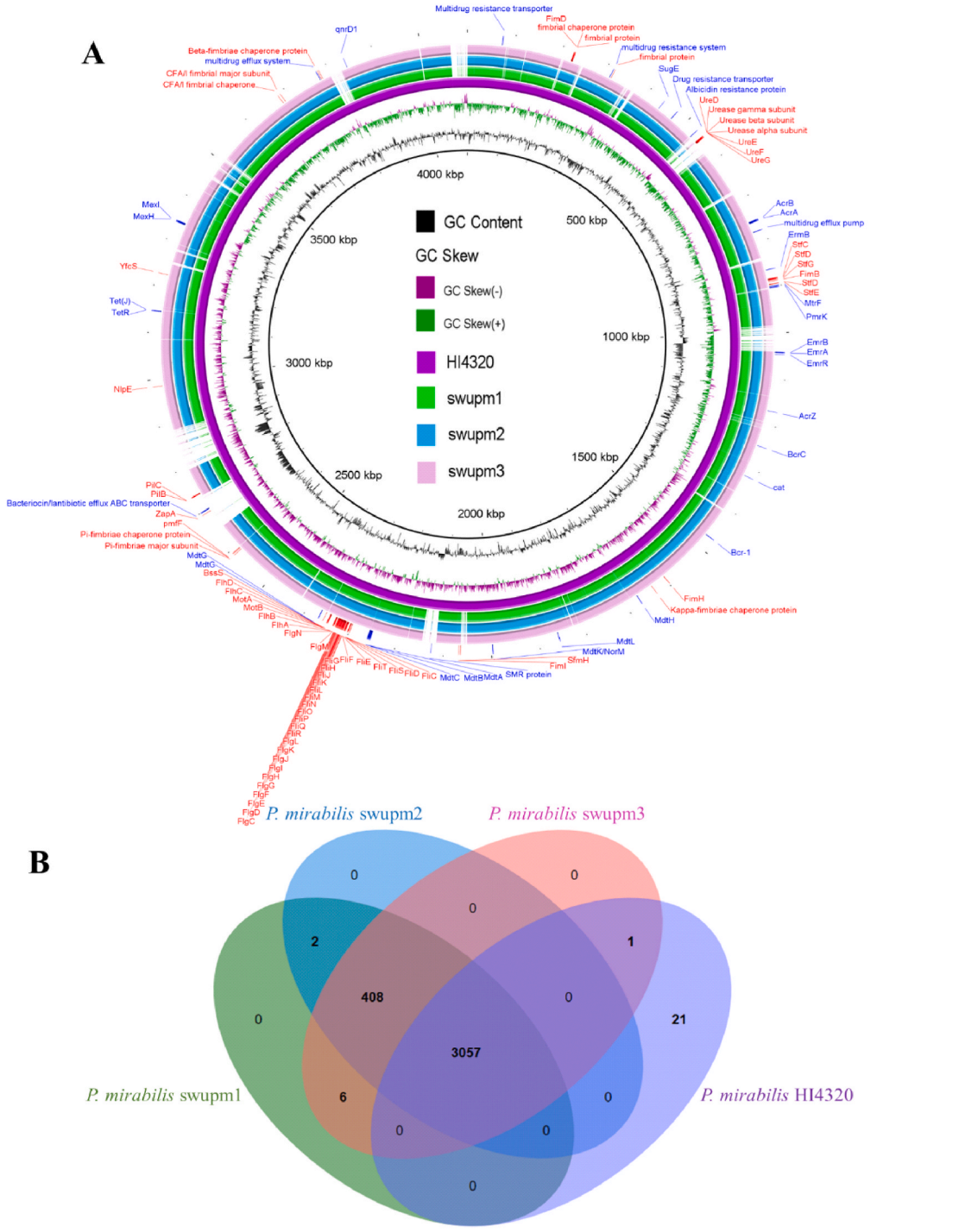

(caption on next page)

Fig. 7. Comparative genome analysis of three *P. mirabilis* strains. (A) Alignment of genome of *P. mirabilis* swupm1, swupm2, swupm3 with the reference *P. mirabilis* HI4320 using BRIG; from inside to outside circles: first circle is GC content, second circle is GC skew, third circle is genome of *P. mirabilis* HI4320, fourth circle is genome of *P. mirabilis* swupm1, fifth circle is genome of *P. mirabilis* swupm2, sixth circle is genome of *P. mirabilis* swupm3, seventh circle is gene annotation where red shows virulence related genes and blue shows antimicrobial resistance related genes. (B) Venn diagram of the orthologous and specific proteins between the three *P. mirabilis* strains and the reference *P. mirabilis* HI4320 using OrthoVenn2. (C) The occurrence pattern of shared orthologous groups among the three *P. mirabilis* strains and the reference *P. mirabilis* HI4320 using OrthoVenn2. (For interpretation of the references to colour in this figure legend, the reader is referred to the Web version of this article.)

P. mirabilis. The fingerprint gives an accurate measurement of each volatile component by cells through depicting different colors: a brighter color represents a higher content. Cells in each row represent the entire compounds in a sample and cells in each column represent the same compound in different samples. As shown in Fig. 6C, *P. mirabilis* treatment caused increase in ethyl propanoate, ethyl acetate, ethanol, formic acid, methyl acetate, 2-methylbutyl acetate, propyl butanoate, oct-1-en-3-ol, 3-methylbutan-1-ol and isoprene. The increase in organic acid, ethanol, ethyl acetate is usually the result of fruit rot caused by microbial metabolites (Pinto, Caputo, Quintieri, de Candia, & Baruzzi, 2017). Moreover, ethyl acetate, ethanol and isoprene have been reported to be volatile components produced by *P. mirabilis* (Thorn, Reynolds, & Greenman, 2011).

All identified volatile components in fresh-cut cantaloupe samples by HS-GC-IMS were summarized in Table 1. Among the 47 volatile components, contents of hexyl acetate, ethyl hexanoate, isopentyl propanoate, isoamyl acetate, ethyl 2-methylbutyrate, butyl acetate, ethyl butyrate, butyl butanoate, isobutyl acetate, iso-propyl propanoate, isopropyl acetate, (e)-3-penten-2-one, 3-hydroxybutan-2-one, acetone, 1-propanol, and ethyl acrylate were found to significantly decrease after *P. mirabilis* treatment. Alcohols, aldehydes, sulphur-containing compounds, acetate esters, other esters are the main flavor components of fresh-cut cantaloupe (Amaro, Beaulieu, Grimm, Stein, & Almeida, 2012). Dissipation of these volatile components also indicated the loss of freshness. This study is the first to provide evidence that *P. mirabilis* can accelerate the decay of fresh-cut fruits and cause loss of flavor components.

3.8. Complete genome sequences of three P. mirabilis strains

To better understand the genetic basis of different phenotypes of three *P. mirabilis* strains, the complete genome sequences of the three *P. mirabilis* strains were obtained and submitted to GenBank of NCBI (accession numbers are in Table 2). Average nucleotide identity (ANI) is proposed to be one of the most robust measurements of genetic relatedness among prokaryotic strains. The pairwise complete genome one-way ANI of the three *P. mirabilis* strains with the reference *P. mirabilis* HI4320 was calculated with values of 98.95% ± 1.37% from 17583 fragments (swupm1), 98.95% ± 1.36% from 17574 fragments (swupm2) and 98.95% ± 1.36% from 17576 fragments (swupm3), respectively. An ANI boundary of 95% has been proposed to distinguish between the genetic relatedness of bacterial species (Ryser, Arias-Roth, Perreten, Irmler, & Bruggmann, 2021). Therefore, strains swupm1, swupm2, and swupm3 were indeed confirmed to be *P. mirabilis*.

Assembly showed that 4 contigs were obtained for *P. mirabilis* strain swupm1, with sizes of 3833071, 4875, 2683, and 2259 bp, respectively. *P. mirabilis* strain swupm2 had 3 contigs with sizes of 3833041, 4942, and 4875 bp, respectively. *P. mirabilis* strain swupm3 had 4 contigs with sizes of 3833058, 4875, 2683, and 2259 bp, respectively. The result indicated that the sizes of chromosome of the three *P. mirabilis* strains were close to each other and the three strains shared the same plasmid with the size of 4875 bp. NCBI BLAST result showed that this common plasmid had the highest identity of 93.17% with one plasmid of *Morganella morganii* FAM24091 and a maximal identity of 88.66% with plasmids from *P. mirabilis* strains. It indicates that although the plasmid is shared by the three *P. mirabilis* strains, it does not widely exist in all *P. mirabilis* strains and may have been transferred from other species. Five CDSs were identified in this common plasmid, including the exonuclease SbcC, the plasmid mobilization relaxosome protein MobC, mobilization protein, the DNA-cytosine methyltransferase, and HaeIII family restriction endonuclease. Except for the QnrD family quinolone resistance pentapeptide repeat protein, CDSs on the other two plasmids all were hypothetical protein with unknown function. Therefore, we deduce that genes related to swarming motility and virulence are located in the chromosome of *P. mirabilis* strains.

3.9. Comparative genome analysis with a clinical reference P. mirabilis strain

In order to explicitly reveal the potential safety risks that the three *P. mirabilis* strains may pose on fresh-cut fruit, comparative genomic analysis of the three *P. mirabilis* strains with a reference *P. mirabilis* HI4320 from a CAUTI patient was conducted. According to circle map of genomes (Fig. 7A), there were some differences between the three *P. mirabilis* strains and the reference *P. mirabilis* HI4320. Core genome of four strains contained 3057 clusters, which involved in 12273 genes (Fig. 7B and C). GO annotation of the core genome demonstrated that 8787 genes belonged to biological process, 568 genes belonged to molecular function, and 273 genes belonged to cellular component. Common virulence associated genes of the four strains included flagellum-dependent cell motility (e.g. *FliS*), flagellum assembly (fe.g. *FlgA*), regulation of flagellum assembly (e.g. *FlhC*), flagellum organization (e.g. *FlgD*), cell adhesion (e.g. fimbrial protein, fimbrial usher protein, fimbrial adhesin), urea catabolic process (e.g. urease), siderophore biosynthetic process (e.g. siderophore biosynthesis protein), siderophore transport (e.g. TonB-dependent siderophore receptor), response to antibiotic (e.g. tetracycline resistance protein, polymyxin resistance protein), etc. As shown in Fig. 7B, 21 specific clusters were owned by *P. mirabilis* HI4320 and involved in functions of phage assembly and attachment, DNA replication, recombination and modification, peptide synthesis, and transposition. It indicates that virulence associated genes of the reference *P. mirabilis* HI4320 located in the core genome but not specific genes. Namely, all virulence associated genes of the reference *P. mirabilis* strain HI4320 were also found in the three *P. mirabilis* strains. Meanwhile, the three *P. mirabilis* strains had accessory genome that consisted of 408 clusters (1232 genes). Among the 1232 genes, virulence associated genes such as those involved in pilus assembly (e.g. fimbrial usher protein), pilus organization (e.g. fimbria periplasmic chaperone), response to antibiotic (e.g. quinolone resistance protein QnrD1), toxin activity (RHS domain-containing protein), zinc ion binding (metalloprotease), etc. were also found. The result indicates that the three *P. mirabilis* strains from fresh-cut fruit had more virulence associated genes than the reference *P. mirabilis* strain HI4320 recovered from a CAUTI patient. The three *P. mirabilis* strains shared 3465 orthologous clusters (13505 genes). Moreover, all genes related to swarming motility and virulence were part of the 13505 genes. *P. mirabilis* strain swupm1 and *P. mirabilis* strain swupm2 shared 2 orthologous clusters (4 genes). *P. mirabilis* strain swupm1 and *P. mirabilis* strain swupm3 shared 6 orthologous clusters (12 genes). It indicates that the genetic differences between the three *P. mirabilis* strains from fresh-cut fruit are small. According to results of comparative genome analysis, we speculate that the three *P. mirabilis* strains from fresh-cut fruit are genetically highly similar, and that their genotypes are close to that of the clinical reference strain, but with even more virulence genes.

Table 3
Genes that contribute to virulence identified in the three *P. mirabilis* strains.

Gene	Function	Classification
FliC	Flagellin	swimming/swarming
FliJ	flagellar protein	swimming/swarming
FliD	flagellar cap protein	swimming/swarming
FliS	flagellar biosynthesis protein	swimming/swarming
FliT	flagellar biosynthesis protein	swimming/swarming
FliO	flagellar biosynthesis protein	swimming/swarming
FliP	flagellar biosynthesis protein	swimming/swarming
FliQ	flagellar biosynthesis protein	swimming/swarming
FliR	flagellar biosynthesis protein	swimming/swarming
FliL	flagellar basal body-associated protein	swimming/swarming
FliK	flagellar hook-length control protein	swimming/swarming
FliE	flagellar hook-basal body complex protein	swimming/swarming
FliF	flagellar M-ring protein	swimming/swarming
FliH	flagellar assembly protein	swimming/swarming
FliG	flagellar motor switch protein	swimming/swarming
FliM	flagellar motor switch protein	swimming/swarming
FliN	flagellar motor switch protein	swimming/swarming
FlgJ	flagellar protein	swimming/swarming
FlgE	flagellar hook protein	swimming/swarming
FlgN	flagellar biosynthesis protein	swimming/swarming
FlgL	flagellar hook-associated protein	swimming/swarming
FlgK	flagellar hook-associated protein	swimming/swarming
FlgI	flagellar P-ring protein	swimming/swarming
FlgH	flagellar L-ring protein	swimming/swarming
FlgG	flagellar basal-body rod protein	swimming/swarming
FlgF	flagellar basal-body rod protein	swimming/swarming
FlgD	flagellar basal-body rod modification protein	swimming/swarming
FlgC	flagellar basal-body rod protein	swimming/swarming
FlgB	flagellar basal-body rod protein	swimming/swarming
FlgA	flagellar basal-body P-ring formation protein	swimming/swarming
FlgM	negative regulator of flagellin synthesis	swimming/swarming
FlhA	flagellar biosynthesis protein	swimming/swarming
FlhB	flagellar biosynthesis protein	swimming/swarming
FlhC	flagellar transcriptional activator	swimming/swarming
FlhD	flagellar transcriptional activator	swimming/swarming
MotB	flagellar motor rotation protein	swimming/swarming
MotA	flagellar motor rotation protein	swimming/swarming
FimI	type 1 fimbriae protein	adherence
FimD	type 1 fimbriae anchoring protein	adherence
StfC	fimbriae usher protein	adherence
StfG	minor fimbrial subunit	adherence
StfE	minor fimbrial subunit	adherence
StfD	periplasmic fimbrial chaperone	adherence
SfmH	fimbriae-like adhesin	adherence
PilB	type IV fimbrial assembly, ATPase	adherence
PilC	type IV fimbrial assembly protein	adherence
YfcS	hypothetical fimbrial chaperone	adherence
–	fimbrial protein	adherence
–	putative fimbrial chaperone protein	adherence
–	type-1 fimbrial protein, A chain	adherence
–	putative minor fimbrial subunit pmfF precursor	adherence
–	periplasmic fimbrial chaperone	adherence
–	type 1 fimbriae regulatory protein, FimB/FimE family	adherence
–	kappa-fimbriae chaperone protein	adherence
–	beta-fimbriae chaperone protein	adherence
–	Pi-fimbriae major subunit	adherence
–	Pi-fimbriae chaperone protein	adherence
–	CFA/I fimbrial chaperone	adherence
–	probable outer membrane fimbrial usher protein	adherence
MrpJ	MrpJ protein	adherence, swimming/swarming
–	urease alpha subunit	urease
–	urease beta subunit	urease
–	urease gamma subunit	urease
UreD	urease accessory protein UreD	urease
UreE	urease accessory protein UreE	urease
UreF	urease accessory protein UreF	urease
UreG	urease accessory protein UreG	urease
BssS	biofilm regulator	biofilm
EfeB	ferrous iron transport peroxidase	iron acquisition
EfeO	ferrous iron transport periplasmic protein	iron acquisition
EfeU	ferrous iron transport permease	iron acquisition
FeoA	ferrous iron transporter-associated protein	iron acquisition
FeoB	ferrous iron transporter	iron acquisition
FeoC	ferrous iron-sensing transcriptional regulator	iron acquisition
FecD	iron(iii) dicitrate transport system permease	iron acquisition
FetA	probable iron export ATP-binding protein	iron acquisition
FetB	probable iron export permease protein	iron acquisition
TonB	ferric siderophore transport system, periplasmic binding protein	iron acquisition
–	siderophore synthetase superfamily, group B	iron acquisition
–	TonB-dependent hemin, ferrichrome receptor	iron acquisition
–	iron-chelator utilization protein	iron acquisition
–	iron compound ABC transporter, ATP-binding protein	iron acquisition
–	ferric iron ABC transporter, ATP-binding protein	iron acquisition
–	ferric iron ABC transporter, iron-binding protein	iron acquisition
–	ferrichrome-iron receptor	iron acquisition
Zur	zinc uptake regulation protein	ion acquisition
ZnuB	zinc ABC transporter, permease protein	ion acquisition
ZnuC	zinc ABC transporter, ATP-binding protein	ion acquisition
ZnuA	zinc ABC transporter, substrate-binding protein	ion acquisition
ModF	putative molybdenum transport ATP-binding protein	ion acquisition
ModA	molybdenum ABC transporter, substrate-binding protein	ion acquisition
ModB	molybdenum ABC transporter permease protein	ion acquisition
ModC	molybdenum ABC transporter ATP-binding protein	ion acquisition
ModD	molybdenum transport system protein	ion acquisition
SitD	manganese ABC transporter, inner membrane permease protein	ion acquisition
SitC	manganese ABC transporter, inner membrane permease protein	ion acquisition
SitB	manganese ABC transporter, ATP-binding protein	ion acquisition
SitA	manganese ABC transporter, periplasmic-binding protein	ion acquisition
MntP	putative manganese efflux pump	ion acquisition
NikE2	nickel ABC transporter, ATP-binding protein	ion acquisition
NikD2	nickel ABC transporter, ATP-binding protein	ion acquisition
NikC2	nickel ABC transporter, permease protein	ion acquisition
NikB2	nickel ABC transporter, permease protein	ion acquisition
NikA2	nickel ABC transporter, substrate-binding protein	ion acquisition
PstS	phosphate ABC transporter, substrate-binding protein	phosphate transport
PstC	phosphate ABC transporter, permease protein	phosphate transport
PstA	phosphate ABC transporter, permease protein	phosphate transport
PstB	phosphate ABC transporter, ATP-binding protein	phosphate transport
PhoU	phosphate transport system regulatory protein	phosphate transport
PhoB	phosphate regulon transcriptional regulatory protein	phosphate transport
PhoR	phosphate regulon sensor protein	phosphate transport
PhoH	phosphate starvation-inducible protein	phosphate transport
–	alkaline phosphatase	phosphate transport
–	low-affinity inorganic phosphate transporter	phosphate transport
–	sodium-dependent phosphate transporter	phosphate transport
ZapA	Z-ring-associated protein	protease
YcbZ	Lon protease	protease
TetR	tetracycline resistance regulatory protein	drug resistance
Tet(J)	tetracycline resistance, MFS efflux pump	drug resistance
PmrK	polymyxin resistance protein	drug resistance
Bcr-1	bicyclomycin resistance protein	drug resistance
Cat	chloramphenicol resistance	drug resistance
qnrD1	quinolone resistance protein	drug resistance
ErmB	multidrug resistance protein	drug resistance
MdtH	multidrug resistance protein	drug resistance
MdtG	multidrug resistance protein	drug resistance
SugE	small multidrug resistance (SMR) efflux transporter	drug resistance
EmrR	multidrug resistance regulator	drug resistance

(*continued on next page*)

Table 3 (*continued*)

Gene	Function	Classification
BcrC	undecaprenyl-diphosphatase, conveys bacitracin resistance	drug resistance
AcrB	multidrug efflux system AcrAB-TolC, inner-membrane proton/drug antiporter	drug resistance
AcrA	multidrug efflux system AcrAB-TolC, membrane fusion component	drug resistance
MtrF	multidrug efflux pump component	drug resistance
EmrB	multidrug efflux system EmrAB-OMF, inner-membrane proton/drug antiporter	drug resistance
EmrA	multidrug efflux system EmrAB-OMF, membrane fusion component	drug resistance
AcrZ	membrane protein associated with AcrAB-TolC multidrug efflux pump	drug resistance
MdtL	multidrug efflux pump	drug resistance
MdtK/ NorM	multidrug efflux transporter	drug resistance
MdtA	multidrug efflux system MdtABC-TolC, membrane fusion component	drug resistance
MdtB	multidrug efflux system MdtABC-TolC, inner-membrane proton/drug antiporter	drug resistance
MdtC	multidrug efflux system MdtABC-TolC, inner-membrane proton/drug antiporter	drug resistance
MexH	multidrug efflux system, membrane fusion component	drug resistance
MexI	multidrug efflux system, inner membrane proton/drug antiporter	drug resistance
–	bacteriocin/lantibiotic efflux ABC transporter	drug resistance
–	multidrug resistance transporter, Bcr/CflA family	drug resistance
–	membrane fusion component of tripartite multidrug resistance system	drug resistance
–	drug resistance transporter, Bcr/CflA family	drug resistance
–	albicidin resistance protein	drug resistance
–	small multidrug resistance family (SMR) protein	drug resistance
–	Na + -driven multidrug efflux pump	drug resistance
–	membrane fusion component of MSF-type tripartite multidrug efflux system	drug resistance

3.10. Virulence genes of the three P. mirabilis strains

In order to elaborately disclose the potential risks of *P. mirabilis* strains from fresh-cut fruit, the types of virulence genes that they contained were analyzed. Common pathogenic strategies employed by *P. mirabilis* include flagella-mediated motility, adherence via fimbriae, urease production, biofilm formation, iron acquisition and immune modulation (Lin et al., 2022). Table 3 shows the genes related to virulence identified in the three *P. mirabilis* strains after gene annotation. Functional flagella are required for both swimming and swarming motility (Lee & Belas, 2015). A total of 37 genes involved in flagellum biosynthesis, function and regulation were identified, including flagellar protein, flagellar biosynthesis protein, flagellar assembly protein, flagellar ring protein, flagellar basal-body protein, flagellar hook protein, flagellar transcriptional activator, flagellar motor switch protein and flagellar motor rotation protein. Adherence of *P. mirabilis* to solid surface (such as epithelium and catheter) is mainly mediated by fimbriae (Bode et al., 2015). A total of 22 genes related to fimbria structure and function were identified, such as fimbrial protein, fimbrial minor subunit, fimbriae major subunit, fimbriae usher protein, fimbriae anchoring protein, fimbriae chaperone protein and fimbriae regulatory protein. The transcriptional regulator MrpJ which plays a key role in regulation of adherence, swimming motility and swarming motility (Bode et al., 2015) was also identified in the three *P. mirabilis* strains. It is surprising that all genes related to swarming motility as mentioned above were identified in all the three *P. mirabilis* strains. There may be other functional regulators leading to phenotypic difference in swarming motility and flagella of the three *P. mirabilis* strains observed above.

In the urinary tract, alkaline pH can lead to precipitation of metal ions (e.g. calcium and magnesium). Urease mediates expression of virulence via the formation of urinary stones as a result of alkalinization of urine upon hydrolyzation of urea to ammonia by urease (Schaffer & Pearson, 2015). In this study, 3 genes of urease subunit and 4 genes of urease accessory protein were identified in the three *P. mirabilis* strains. Biofilm is mainly composed of polysaccharides, proteins and nucleic acids. *P. mirabilis* can form crystalline biofilm, which blocks urine flow through the catheter and protects the pathogen from host defenses and antibiotic treatment (Durgadevi et al., 2020). A biofilm regulator gene was identified in the three *P. mirabilis* strains. Pathogens can acquire free iron from the host by different iron-acquisition systems. In the three *P. mirabilis* strains, siderophore-based systems, ferrous iron transporters and metal-type ABC transporters were identified. Siderophore identified in *P. mirabilis* can bind and solubilize Fe^{3+} mediated by the receptor TonB. FeoA and FeoB are Fe^{2+} transport proteins, and FeoC, EfeO, EfeB, EfeU were involved in ferrous iron transport. It means that the three *P. mirabilis* strains have a strong iron acquisition capability within the host. ZnuACB is a functional zinc uptake system and zinc uptake provides a competitive advantage for the pathogens. In addition, zinc is needed for the functions of other virulence factors (e.g. flagella and zapA) of *P. mirabilis* (Schaffer & Pearson, 2015). Except for iron and zinc, the three *P. mirabilis* strains also have the abilities to acquire molybdenum, manganese, and nickel, in order to enhance their competitive advantage. Four genes associated with phosphate transport (PstSCAB), and a negative transcriptional regulator PhoU, form the *pst* operon. The *pst* operon and an alkaline phosphatase gene were identified in the three *P. mirabilis* strains, and could contribute to UTI (Schaffer & Pearson, 2015). Genes of ZapA metalloprotease and Lon protease were also identified in the three *P. mirabilis* strains, which compromise host immune and influence the swarming motility of the pathogen. Undoubtedly, it is necessary to pay close attention to the safety risks of fresh-cut fruit polluted by *P. mirabilis*.

Drug resistance in *P. mirabilis* aids the difficulty in treating infections. As shown in Table 3, resistance genes of tetracycline, polymyxin, bicyclomycin, chloramphenicol, and quinolone were identified. Moreover, a large number of multidrug resistance genes were found in the three *P. mirabilis* strains, including those encoding multidrug resistance protein, multidrug efflux pump, multidrug efflux transporter, multidrug efflux system and multidrug resistance regulator.

4. Conclusion

The three *P. mirabilis* strains isolated from fresh-cut fruits differ in swarming motility, growth rate and biofilm-formation characteristics, but they had similar cell morphology and genome composition. The three *P. mirabilis* strains had strong *in vivo* toxicity that cell density of all strains $\geq$100 bacteria/insect can lead to 100% death of *G. mellonella*. Namely, *P. mirabilis* may have variable morphology, but exhibit similar toxicity. In fresh-cut fruits, *P. mirabilis* can accelerate the decay of fruit and lead to loss of flavor components, which results from accelerated degradation of fruits components with increased growth of total bacteria. Genome analysis showed that the three *P. mirabilis* strains exhibited high genetic similarity with the clinical strain *P. mirabilis* HI4320, but they had more virulence associated genes than *P. mirabilis* HI4320. The different abilities of these three *P. mirabilis* strains to cause food spoilage and virulence in wax worm need further investigation since comparative genomic analysis failed to identify any potential genetic mechanisms that contribute to these variations. Data from this study confirmed that *P. mirabilis* with high virulence could lead to rapid decay of fresh-cut fruits and warrants further study to evaluate its effect on food safety and public health.

Author contributions

Author 1: Lanhua Yi: Acquired the financial support for the project leading to this publication, collected the data, wrote and revised the Manuscript.

Author 2: Ping Zeng: Collected the data, wrote and revised the Manuscript.

Author 3: Jitao Tang: Collected the data.

Author 4: Junhe Ren: Collected the data.

Author 5: Kaifang Zeng: Acquired the financial support for the project leading to this publication. Conceived and designed the analysis.

Author 6: Sheng Chen: Acquired the financial support for the project leading to this publication. Conceived and designed the analysis, as well as revised the Manuscript.

Declaration of competing interest

We declare that we do not have any personal, financial, commercial or associative interest that represents a conflict of interest in connection with the work submitted.

Data availability

Data will be made available on request.

Acknowledgments

This research was supported by the Fundamental Research Funds for the Central Universities (Grant No. SWU-KT22047), the Innovation and Entrepreneurship Training Program for College Students (X202210635097), the National Natural Science Foundation of China (No. 32102032) and the Entrepreneurship and Innovation Support Program for Overseas Students in Chongqing (No. CX2021096).

References

Amaro, A. L., Beaulieu, J. C., Grimm, C. C., Stein, R. E., & Almeida, D. P. F. (2012). Effect of oxygen on aroma volatiles and quality of fresh-cut cantaloupe and honeydew melons. *Food Chemistry, 130*(1), 49–57.

Armbruster, C. E., Mobley, H. L. T., & Pearson, M. M. (2018). Pathogenesis of *Proteus mirabilis* infection. *EcoSal Plus, 8*(1). ESP-0009-2017.

Banville, N., Browne, N., & Kavanagh, K. (2012). Effect of nutrient deprivation on the susceptibility of *Galleria mellonella* larvae to infection. *Virulence, 3*(6), 497–503.

Bode, N. J., Debnath, I., Kuan, L., Schulfer, A., Ty, M., & Pearson, M. M. (2015). Transcriptional analysis of the MrpJ network: Modulation of diverse virulence-associated genes and direct regulation of mrp fimbrial and flhDC flagellar operons in *Proteus mirabilis*. *Infection and Immunity, 83*(6), 2542–2556.

Chadwick, J. S. (1967). Some aspects of immune responses in insects. *Society for In Vitro Biology, 3*, 120–128.

Chadwick, J. S. (1971). Effects of immunization on LD50 of two pathogens of *Galleria mellonella*. *Journal of Invertebrate Pathology, 18*(1), 117–120.

Durgadevi, R., Abirami, G., Alexpandi, R., Nandhini, K., Kumar, P., Prakash, S., et al. (2019). Explication of the potential of 2-hydroxy-4-methoxybenzaldehyde in hampering uropathogenic *Proteus mirabilis* crystalline biofilm and virulence. *Frontiers in Microbiology, 10*, 2804.

Durgadevi, R., Abirami, G., Swasthikka, R. P., Alexpandi, R., Pandian, S. K., & Ravi, A. V. (2020). Proteomic analysis deciphers the multi-targeting antivirulence activity of tannic acid in modulating the expression of MrpA, FlhD, UreR, HpmA and Nrp system in *Proteus mirabilis*. *International Journal of Biological Macromolecules, 165*, 1175–1186.

Filipiak, A., Chrapek, M., Literacka, E., Wawszczak, M., Gluszek, S., Majchrzak, M., et al. (2020). Pathogenic factors correlate with antimicrobial resistance among clinical *Proteus mirabilis* strains. *Frontiers in Microbiology, 11*, Article 579389.

Fpds, A., Kmf, B., Lldf, A., Rdsc, A., Rcb, C., Lldo, B., et al. (2021). Effects of sub-lethal doses of nisin on the virulence of *Salmonella enterica* in *Galleria mellonella* larvae - ScienceDirect. *Research in Microbiology*, Article 103836. RESMIC.

Freitas, L., Silva, F., Fernandes, K. M., Carneiro, D. G., & Vanetti, M. (2021). The virulence of *Salmonella enteritidis* in *Galleria mellonella* is improved by N-dodecanoyl-homoserine lactone. *Microbial Pathogenesis, 152*, Article 104730.

Gong, Z. L., Bai, F., Ng'ambi, D., Shi, X. L., & Cao, H. (2018). Effect of extracellular conditions on diarrheal *Proteus mirabilis in vitro*: A preliminary study on virulence of *Proteus mirabilis* from a food poisoning in shenzhen, China. *International Journal of Infectious Diseases, 73*, 116-116.

Guo, S., Zhao, X., Ma, Y., Wang, Y., & Wang, D. (2022). Fingerprints and changes analysis of volatile compounds in fresh-cut yam during yellowing process by using HS-GC-IMS. *Food Chemistry, 369*, Article 130939.

Jiang, X., Yu, T., Liu, L., Li, Y., Zhang, K., Wang, H., et al. (2017). Examination of quaternary ammonium compound resistance in *Proteus mirabilis* isolated from cooked meat products in China. *Frontiers in Microbiology, 8*, 2417.

Lee, Y.-Y., & Belas, R. (2015). Loss of FliL alters *Proteus mirabilis* surface sensing and temperature-dependent swarming. *Journal of Bacteriology, 197*(1), 159–173.

Lin, W.-Y., Lee, Y.-J., Yu, P.-H., Tsai, Y.-L., She, P.-Y., Li, T.-S., et al. (2022). The QseEF two-component system-GlmY small RNA regulatory pathway controls swarming in uropathogenic *Proteus mirabilis*. *International Journal of Molecular Sciences, 23*(1), 487.

O'May, C., Amzallag, O., Bechir, K., & Tufenkji, N. (2016). Cranberry derivatives enhance biofilm formation and transiently impair swarming motility of the uropathogen *Proteus mirabilis* HI4320. *Canadian Journal of Microbiology, 62*(6), 464–474.

de Oliveira, W. D., Lopes Barboza, M. G., Faustino, G., Yamanaka Inagaki, W. T., Sanches, M. S., Takayama Kobayashi, R. K., et al. (2021). Virulence, resistance and clonality of *Proteus mirabilis* isolated from patients with community-acquired urinary tract infection (CA-UTI) in Brazil. *Microbial Pathogenesis, 152*, Article 104642.

Pinto, L., Caputo, L., Quintieri, L., de Candia, S., & Baruzzi, F. (2017). Efficacy of gaseous ozone to counteract postharvest table grape sour rot. *Food Microbiology, 66*, 190–198.

Ryser, L. T., Arias-Roth, E., Perreten, V., Irmler, S., & Bruggmann, R. (2021). Genetic and phenotypic diversity of *Morganella morganii* isolated from cheese. *Frontiers in Microbiology, 12*, Article 738492.

Sanches, M. S., da Silva, C. R., Silva, L. C., Montini, V. H., Lopes Barboza, M. G., Migliorini Guidone, G. H., et al. (2021). *Proteus mirabilis* from community-acquired urinary tract infections (UTI-CA) shares genetic similarity and virulence factors with isolates from chicken, beef and pork meat. *Microbial Pathogenesis, 158*, Article 105098.

Schaffer, J. N., & Pearson, M. M. (2015). *Proteus mirabilis* and urinary tract infections. *Microbiology Spectrum, 3*(5). UTI-0017-2013.

Thorn, R. M. S., Reynolds, D. M., & Greenman, J. (2011). Multivariate analysis of bacterial volatile compound profiles for discrimination between selected species and strains *in vitro*. *Journal of Microbiological Methods, 84*(2), 258–264.

Wang, Y., Zhang, S., Yu, J., Zhang, H., Yuan, Z., Sun, Y., et al. (2010). An outbreak of *Proteus mirabilis* food poisoning associated with eating stewed pork balls in brown sauce, Beijing. *Food Control, 21*(3), 302–305.

Wick, R. R., Judd, L. M., Gorrie, C. L., & Holt, K. E. (2017). Unicycler: Resolving bacterial genome assemblies from short and long sequencing reads. *PLoS Computational Biology, 13*(6), Article e1005595.

Yeh, H.-Y., Line, J. E., & Hinton, A., Jr. (2018). Molecular analysis, biochemical characterization, antimicrobial activity, and immunological analysis of *Proteus mirabilis* isolated from broilers. *Journal of Food Science, 83*(3), 770–779.

Yi, L., Chen, S., Li, G., Ren, J., Zhou, R., & Zeng, K. (2022). Prevalence of antibiotic resistance pathogens in online fresh-cut fruit from Chongqing, China and controlling *Enterococcus faecalis* by bacteriocin GF-15. *LWT-Food Science and Technology, 165*, Article 113678.

Yi, L. H., Qi, T., Hong, Y., Deng, L. L., & Zeng, K. F. (2020). Screening of bacteriocin-producing lactic acid bacteria in Chinese homemade pickle and dry-cured meat, and bacteriocin identification by genome sequencing. *LWT-Food Science and Technology, 125*, Article 109177.

Yuan, F., Huang, Z., Yang, T., Wang, G., Li, P., Yang, B., et al. (2021). Pathogenesis of *Proteus mirabilis* in catheter-associated urinary tract infections. *Urologia Internationalis, 105*(5–6), 354–361.